Proceedings of the International Conference on Fluid Flow and Thermal Science (ICFFTS'20)
Virtual Conference – September 9-10, 2020
Paper No. 130

Two Approaches to Mathematical Modelling of Heating/Evaporation of a Multi-component Liquid Film

Ming Jia
Key Laboratory of Ocean Energy Utilization and Energy Conservation of the Ministry of Education
Dalian University of Technology,
Dalian 116024, PR China
jiaming@dlut.edu.cn

Yanzhi Zhang
Institute for Energy Research,
Jiangsu University
Zhenjiang 212013, PR China
zhangyanxzhi@ujs.edu.cn

Oyuna Rybdylova
Advanced Engineering Centre
School of Computing, Engineering and Mathematics
University of Brighton
Brighton, BN2 4GJ, UK
O.Rybdylova@brighton.ac.uk

Sergei S. Sazhin *
Advanced Engineering Centre
School of Computing, Engineering and Mathematics
University of Brighton
Brighton BN2 4GJ, UK
S.Sazhin@brighton.ac.uk

Abstract - Two numerical algorithms for modelling multi-component liquid film heating/evaporation are compared. Both algorithms are based on the solutions of one-dimensional heat transfer/species diffusion equations describing the processes in the liquid film. One of these algorithms is based on the fully numerical solutions of these equations, while the second one is based on their analytical solutions at each time step. The predictions of both algorithms are compared for the case of a 50%/50% hexadecane/heptane film under typical Diesel engine conditions. The agreement between the time evolution of thickness and surface/average temperatures of the film, predicted by both algorithms, appears to be rather close. This allows us to recommend both algorithms for practical engineering applications.

Keywords: Film of liquid; Multi-component; Evaporation; Heating; Internal combustion engines; Numerical solutions

Nomenclature

c	specific heat capacity
D	diffusion coefficient
f_n	parameter introduced in (15)
h	convection heat transfer coefficient
h_m	convection mass transfer coefficient
h_0	$h\delta_0/k_l$
k	thermal conductivity
L	specific heat of evaporation
$\mathrm{L}e$	Lewes number
M	molar mass
$\dot{m}_f$	evaporation mass flux
p	pressure
Pr	Prandtl number
q_n	parameter introduced in Equation (15)
q_{Yn}	parameter introduced in Equation (16)
R_u	universal gas constant
Sc	Schmidt number
t	time

Greek symbols

δ	film thickness
$\Delta\delta_0$	change in film thickness
Δt	time step
ϵ_i	parameter defined by (10)
κ	thermal diffusivity
$\kappa_{\delta 0}$	$k_l/(c_l\rho_l\delta_0^2)$
λ_n	eigenvalues
μ	dynamic viscosity
ρ	density

Subscripts

a	ambient
eff	effective
e	evaporation
g	gas
i	species
l	liquid phase
p	constant pressure

T	temperature	ref	reference
u	parameter defined by Equation (16)	s	surface of the film
v_n	eigenfunction	v	vapour phase
x	distance from the wall	w	wall
X	x/δ_0 or molar fraction	0	value at the beginning of a time step or initial value
Y	mass fraction	1	value at the end of a time step

1 Introduction

The practical importance of modelling of multi-component film heating/evaporation in engineering/environmental/pharmaceutical applications, including those in internal combustion (IC) engines, has been extensively discussed by many authors (e.g. [1], [2]. [8], [5]). Perhaps the most comprehensive numerical model of these processes is described in [8]. The model suggested in this paper assumes that film is thin and heating and evaporation processes can be described by 1D heat transfer/species diffusion equations. These authors used the numerical solutions of these equations.

An alternative approach to the problem was later proposed in [5]. The model described in this paper was based on assumptions similar to those used in [8]. In contrast to [8], however, the authors of [5] used the analytical rather than numerical solutions to the underlying partial differential equations. These analytical solutions were used at each time step and were incorporated into the general numerical scheme. Both models suggested in [8] and [5] were validated using the available experimental data.

The aim of this paper is to perform a verification of both models using direct comparison of their predictions referring to a typical realistic case of multi-component film heating/evaporation. This will give additional confidence in the suitability of both models for practical engineering applications.

Equations/approximations used in both models are summarised in Section 2. The numerical algorithms used in these models are outlined in Section 3. Comparisons between the predictions of both models are presented in Section 4. The key outcomes of the paper are summarised in Section 5.

2 Equations and approximations

The equation for the temperature in the liquid film is presented as:

$$\frac{\partial T}{\partial t} = \kappa_\mathrm{l} \frac{\partial^2 T}{\partial x^2}, \tag{1}$$

where x is the distance from the wall, $\kappa_\mathrm{l} = k_\mathrm{l}/(c_\mathrm{l}\rho_\mathrm{l})$ is the thermal diffusivity; c_l, k_l, and ρ_l are the specific heat capacity, thermal conductivity, and density, respectively.

Following [2], the liquid temperature at the wall is assumed to be constant; it is equal to the temperature of the wall: $T(x = 0, t) = T_\mathrm{w}$ (Dirichlet BC). The boundary condition at the liquid film surface ($x = \delta$) is presented as [2]:

$$h(T_\mathrm{eff} - T_\mathrm{s}) = k_\mathrm{l} \left.\frac{\partial T}{\partial x}\right|_{x=\delta-0} \tag{2}$$

where

$$T_{eff} = T_\mathrm{g} + \frac{\rho_\mathrm{l} L \dot{\delta}_e}{h}, \tag{3}$$

$\dot{\delta}_e$ is controlled by evaporation (additional subscript $_e$), L is the specific enthalpy of evaporation, T_s and T_g are film surface and gas temperatures, h is the convection heat transfer coefficient.

Using the above-mentioned boundary and initial conditions, the analytical solution to Equation (1) for each time step was obtained in [5]. It is presented in Appendix 1.

The value of h is assumed to be constant. Following [6], the Chilton-Colburn analogy was used to estimate the mass transfer coefficient h_m:

$$h_{\mathrm{m}} = \frac{h}{\rho_{\mathrm{g}} c_{p\mathrm{g}}} \mathrm{Le}^{-2/3}, \tag{4}$$

where Le is the Lewis number ($\mathrm{Le} = \mathrm{Sc}/\mathrm{Pr}_{\mathrm{g}}$), $\mathrm{Sc} = \mu_{\mathrm{g}}/\rho_{\mathrm{g}} D_{\mathrm{g}}$ is the Schmidt number, D_{g} is the diffusivity of gas. The diffusivities of all components are assumed to be the same (for multi-component vapour).

The surface evaporation mass flux is estimated as [7]:

$$\dot{m}_{\mathrm{f}} = h_{\mathrm{m}} (\rho_{\mathrm{v}s} - \rho_{\mathrm{v}g}), \tag{5}$$

where $\rho_{\mathrm{v}s}$ and $\rho_{\mathrm{v}g}$ are the densities of vapour at the surface of the film and in gas. It is assumed that $\rho_{\mathrm{v}g} = 0$. The value of $\dot{\delta}_e$ is found as:

$$\dot{\delta}_e = -\left|\frac{\dot{m}_{\mathrm{f}}}{\rho_l(\overline{T})}\right|, \tag{6}$$

where $\overline{T}$ is the film average temperature, ρ_{l} is the liquid density.

The equation for species diffusion in the liquid film is presented as:

$$\frac{\partial Y_{\mathrm{l},i}}{\partial t} = D_{\mathrm{l}} \frac{\partial^2 Y_{\mathrm{l},i}}{\partial x^2}, \tag{7}$$

where D_{l} is the diffusion coefficient of liquid species. The following boundary conditions are used for solving Equation (7):

$$D_{\mathrm{l}} \frac{\partial Y_{\mathrm{l},i}}{\partial x}\bigg|_{x=\delta-0} = |\dot{\delta}_e| \left(Y_{\mathrm{l},i}\big|_{x=\delta} - \epsilon_i \right), \tag{8}$$

$$\frac{\partial Y_{\mathrm{l},i}}{\partial x}\bigg|_{x=0} = 0, \tag{9}$$

where $\left|\dot{\delta}_e\right| = h_m \sum_{i=1}^{i=N} \rho_{\mathrm{v}s,i}/\rho_{\mathrm{l}}$, $\rho_{\mathrm{v}s,i}$ are surface densities of the vapour species, N is the total number of species,

$$\epsilon_i = \frac{Y_{\mathrm{v}s,i}}{\sum_{i=1}^{i=N} Y_{\mathrm{v}s,i}} = \frac{\rho_{\mathrm{v}s,i}}{\sum_{i=1}^{i=N} \rho_{\mathrm{v}s,i}}, \tag{10}$$

$Y_{\mathrm{v}s,i}$ are the mass fraction of vapour species at the film surface. The initial condition is $Y_{\mathrm{l},i}(t=0) = Y_{\mathrm{l}0,i}$. $\dot{m}_{\mathrm{f}}$ is positive, but $\dot{\delta}_e$ is negative. We assume that $\epsilon_i = const$ during a time step [5].

Using the above-mentioned boundary and initial conditions, the analytical solution to Equation (7) at each time step was obtained in [5]. It is presented in Appendix 1.

The partial pressures of surface vapour components are obtained from Raoult's law:

$$p_{\mathrm{v}s,i} = X_{\mathrm{l}s,i} p^*_{\mathrm{v},i}, \tag{11}$$

where $X_{\mathrm{l}s,i}$ are the molar fractions of the surface liquid species, $p^*_{\mathrm{v},i}$ are the partial surface species vapour pressures when $X_{\mathrm{l},i} = 1$. $p^*_{\mathrm{v},i}$ are obtained from the Pitzer expansion with Ambrose and Walton expressions for the functions used in this expansion [3].

The values of $\rho_{\mathrm{v}s,i}$ are estimated as:

$$\rho_{\mathrm{v}s,i} = \frac{p_{\mathrm{v}s,i} M_i}{R_{\mathrm{u}} T_{\mathrm{s}}}, \tag{12}$$

where R_{u} and T_{s} are the universal gas constant and the temperature at the film surface. The species evaporation flux is estimated as (cf. Formula (5)):

$$\dot{m}_{\mathrm{f}i} = h_{\mathrm{m}}\rho_{\mathrm{v}s,i}, \tag{13}$$

where h_{m} is assumed to be the same for all species.

The change in thickness of a film due to evaporation $-\Delta t\frac{|\dot{m}_{\mathrm{f}i}|}{\rho(\overline{T})}$ and thermal swelling $\left[\frac{\rho(\overline{T}_0)}{\rho(\overline{T}_1)}-1\right]\delta_0$ is estimated as:

$$\Delta\delta_0 = -\Delta t\frac{|\dot{m}_{\mathrm{f}i}|}{\rho(\overline{T}_0)} + \left[\frac{\rho(\overline{T}_0)}{\rho(\overline{T}_1)}-1\right]\delta_0, \tag{14}$$

where subscripts 0 (1) denote values at the start (end) of the time step Δt, and $\rho(\overline{T})$ is the liquid density calculated using the average film temperature. Liquid thermodynamic and transport properties are calculated at average liquid film composition and temperature. The properties of the mixture are assumed to be the same as of air at the reference temperature $T_{\mathrm{ref}} = (2/3)T_s + (1/3)T_a$, where T_s (T_a) is the surface film (ambient air) temperature. Partial vapour component pressures and specific enthalpies of evaporation are estimated at the film surface temperature.

3 Solution algorithms

3.1 Algorithm used in [8]

A one-dimensional numerical model was implemented in-house code. The details can be found in [8]. These are the main steps of the calculation process.

Firstly, the distributions of temperature and species mass fractions within the liquid film are initialised using the initial and boundary conditions. The partial pressures of species and their vapour densities at the film surface are calculated using Equations (11) and (12), and the species evaporation rate is determined by Equation (13). Then the transport/thermodynamic properties of the mixtures of the liquid species are calculated. Furthermore, the temperature and species mass fractions in the liquid film for the next time step are obtained by numerically solving Equations (1) and (7). Finally, the film thickness at the next time step is calculated using Equation (14).

For the numerical solution of Equations (1) and (7), we used an implicit finite difference approach. In this approach, the central-differencing scheme for space and the forward-Euler scheme for time were adopted. We used a uniform grid of 100 cells across the film and a time step of 10^{-5} s. It was shown that the results remain almost the same with further refinement of these parameters. As the grid number was kept constant in the calculation, the grid size continually shrank during the evaporation process.

3.2 Algorithm used in [5]

The key steps used in this algorithm are described in [5]. In what follows, the main structure of the algorithm is summarised.

The analysis starts by assuming that the initial distribution of temperature and species (or the distributions inferred from the previous time step) in the film are functions of the distance from the wall. Then partial pressures of species and their molar fractions are calculated using Equation (11). Species evaporation rates (ϵ_i) are calculated based on Equation (10). Then transport and thermodynamic properties of the mixtures of liquid species are calculated. Next, the temperature and species distribution inside the film are calculated based on Expressions (15) and (16) (40 terms in the series in (15) and 100 terms in the series in (16) are used). This step allowed us to obtain the temperature and species distributions inside and at the surface of the film at the end of the time step.

Finally, the change in the thickness of the film is obtained using Equation (14). The results presented in the paper were obtained using time step size 10 μs and 200 uniform layers in the film. The descretisation of the space in the film is required for calculating parameters q_n in Expression (15) and parameters q_{Yn} in Expression (16).

Note that in both algorithms special care is applied to prevent the unphysical scenario where film surface temperature approaches or exceeds the critical temperatures of the components. None of the models is strictly applicable in this case.

4 Results

4.1 Formulation of the problem

We consider the same problem of heating/evaporation of a 50%/50% heptane/hexadecane film as discussed in Section 5.2 of [5]. The input parameters presented in Table 1 are used in calculations. Transport and thermodynamic properties, used in calculations, are the same as in [5].

Table 1: Values of parameters used in our calculations.

Ambient temperature, T_g	900 K
Ambient pressure, p_g	60 bar
Wall temperature, T_w	500 K
Initial film temperature, T_0	363 K
Initial film thickness, δ_0	20 μm
Convection heat transfer coefficient, h	2000 W/(m^2 K)

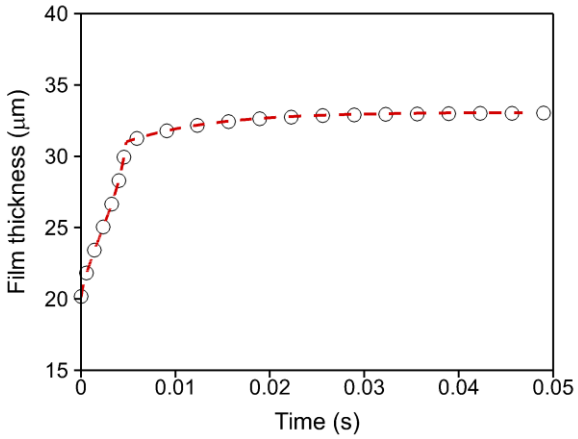

Fig. 1: The film thickness predicted by the algorithms described in [8] (dashed curve) and in [5] (circles) for the parameters shown in Table 1 (non-evaporating case).

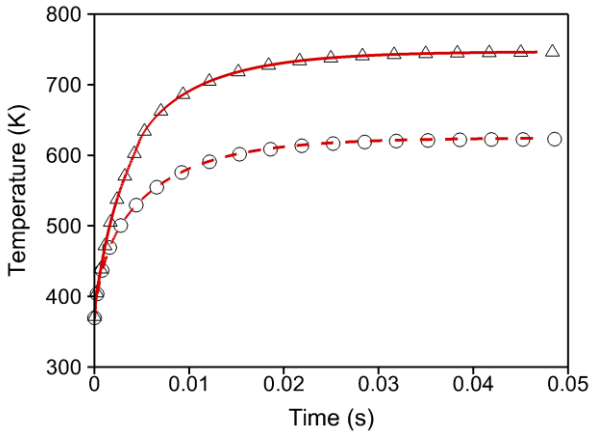

Fig. 2: The surface (average) temperature predicted by the algorithms described in [8] (solid curve (dashed curve)) and in [5] (triangles (circles)) for the values of input parameters shown in Table 1 (non-evaporating case).

4.2 Comparison of the results (non-evaporating case)

We start the comparison between the predictions of the two algorithms for the simplest artificial case when the effects of evaporation are not taken into account. The values of the liquid film thickness, and temperature versus time predicted by both algorithms are shown in Figures 1 and 2. The agreement between the predictions of the algorithms appears to be almost perfect which gives us confidence in the reliability of both these codes for this particular case.

Note that unrealistically high values of film temperatures (surface and average), predicted by both codes and shown in Figure 2, are attributed to the absence of evaporation, which plays the role of natural limiter of these temperatures. The increase in film thickness shown in Figure 1 is the result of thermal swelling. This thermal swelling naturally leads to a decrease in liquid density.

4.3 Comparison of the results (evaporating case)

At the next step, we consider a realistic case when evaporation of the film components (heptane and hexadecane), and hence their mutual diffusion in the film, are taken into consideration.

The values of the liquid film thickness and temperature versus time predicted by both algorithms are shown in Figures 3 and 4. The agreement between the predictions of both algorithms appears to be very close for most times. In contrast to the results shown in Figures 1 and 2, however, there is a noticeable difference between the film thicknesses predicted by the algorithms at times close to 0.02 s.[1] Also, the lifetime of the film predicted by the algorithm described in [8] is slightly longer than the one predicted by the algorithm described in [5].

The plots of mass fraction of heptane for the same input parameters as in Figures 3 and 4 are shown in Figure 5. Similarly to the cases presented in Figures 3 and 4, the predictions of both algorithms shown in Figure 5 are rather close, although there is a visible deviation between them at times close to about 0.015 s. Figure 5 shows that both algorithms predict a complete evaporation of heptane by about 0.02 s. This leads to a rapid decrease in the film thickness shown in Figure 3, after the initial thermal swelling.

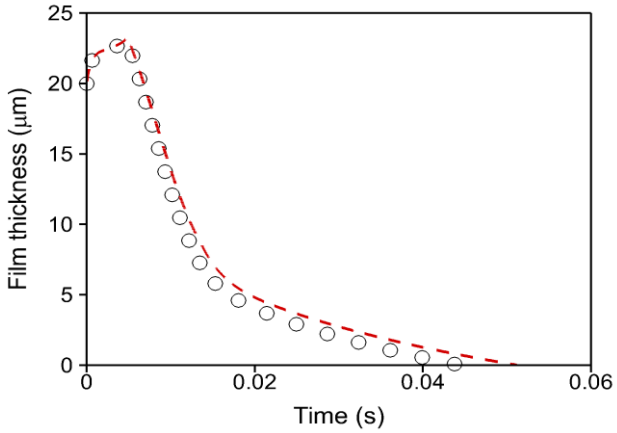

Fig. 3: The film thickness predicted by the algorithms presented in [8] (dashed curve) and in [5] (circles) for the values of parameters shown in Table 1 (evaporating case).

[1] Note that there are some slight differences between the assumptions used in [5] and those used in the current paper. Firstly, the liquid diffusivity model used in the current paper is based on Expressions (51) and (52) of [4] for viscosity, while a rather crude model for this parameter was used in [5]. Secondly, our analysis is based on the assumption that Le=1, to be consistent with the corresponding assumption used in [8]. These differences led to slight differences between the plots shown in Figures 3 and 5 of [5] and the above-mentioned Figures 3 and 4.

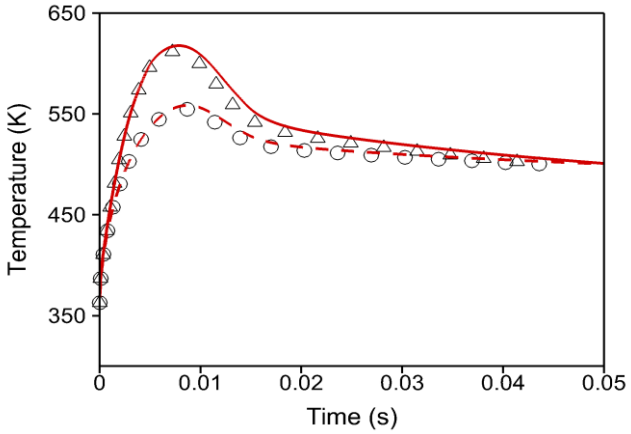

Fig. 4: The surface (average) temperature predicted by the algorithms presented in [8] (solid curve (dashed curve)) and in [5] (triangles (circles)) for the values of parameters shown in Table 1 (evaporating case).

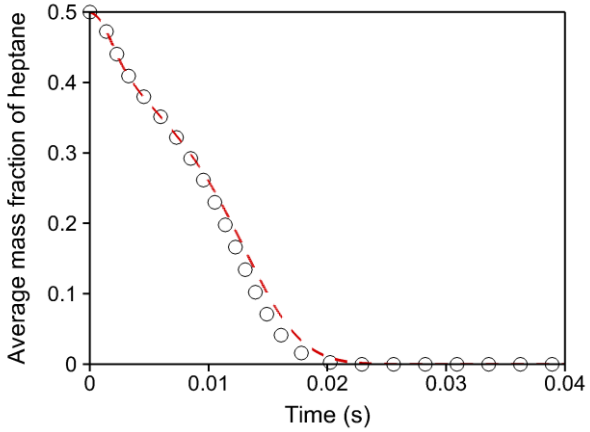

Fig. 5: Average heptane mass fraction predicted by the algorithms presented in [8] (dashed curve) and in [5] (circles) for the parameters shown in Table 1 (evaporating case).

The reasons for the above-mentioned small deviations between the predictions of the algorithms described in [8] and [5] are not fully clear to us. We do not think, however, that this is important with regard to the practical application of these codes, as the deviations are much smaller than the typical measurement errors of these parameters. This allows us to conclude that both of the algorithms described in [8] and [5] can be used with confidence for the analysis of practical engineering film heating/evaporation.

5 Conclusions

Two previously developed numerical algorithms for modelling multi-component liquid film heating and evaporation are described. Both algorithms are based on the assumption that the film is sufficiently thin that the gradients of temperature and species mass fractions in the direction parallel to the flat wall can be ignored compared with those in the direction perpendicular to it. The difference between these algorithms lies in the way in which temperature and species diffusion equations in the film are solved. In the algorithm described in [8] these equations are solved numerically, while in the algorithm described in [5] they are solved analytically at each time step. These analytical solutions are incorporated into the general numerical scheme.

Both algorithms are applied to the analysis of heating/evaporation of a 50%/50% hexadecane/heptane film under conditions typical of Diesel engines. At first an idealised case of a non-evaporating film is considered, then the analysis is refocused on the more realistic case of an evaporating film. For a non-evaporating film the agreement between the

predicted film thicknesses and average/surface film temperatures by the two algorithms appears to be almost perfect. For an evaporating film, this agreement appears to be less close, but the difference between the predictions of these algorithms is much smaller than the typical measurement errors of experimental measurements. This allows us to recommend both algorithms for practical engineering applications.

Acknowledgements

The financial support by the EPSRC (UK) [grants EP/R012024/1 and EP/M002608/1], the National Natural Science Foundation of China [grants 91641117 and 51961135105], and the Natural Science Foundation of Jiangsu Province, China [grant SBK2019040799] are gratefully acknowledged.

References

[1] A. Faghri and Y. Zhang. *Transport Phenomena in Multiphase Systems*. Elsevier, Amsterdam, 2006.

[2] Song Liye, Zhang Weizheng, Zhang Tien, and Qin Zhaoju. A new approach to transient evaporating film heating modeling based on analytical temperature profiles for internal combustion engines. *International Journal of Heat and Mass Transfer*, 81:465–469, 2015.

[3] B. E. Poling, J. M. Prousnitz, and J. O'Connell. *The Properties of Gases and Liquids*. McGraw-Hill, New York, 2001.

[4] S. S. Sazhin, M. Al Qubeissi, R. Nasiri, V. M. Gunko, A. E. Elwardany, F. Lemoine, F. Grisch, and M. R. Heikal. A multi-dimensional quasi-discrete model for the analysis of diesel fuel droplet heating and evaporation. *Fuel*, 129:238–266, 2014.

[5] S. S. Sazhin, O. Rybdylova, and C. Crua. A mathematical model for heating and evaporation of a multi-component liquid film. *International Journal of Heat and Mass Transfer*, 117:252–260, 2018.

[6] H.-J. Steeman, A. Janssens, and M. De Paepe. On the applicability of the heat and mass transfer analogy in indoor air flows. *International Journal of Heat and Mass Transfer*, 52:1431–1442, 2009.

[7] P. T Tsilingiris. Modeling heat and mass transport phenomena at higher temperatures in solar distillation systems - the Chilton-Colburn analogy. *Solar Energy*, 84:308–317, 2010.

[8] Yanzhi Zhang, Ming Jia, Ping Yi, Hong Liu, and Maozhao Xie. An efficient liquid film vaporization model for multi-component fuels considering thermal and mass diffusions. *Applied Thermal Engineering*, 112:534 – 548, 2017.

Appendix 1

The solution to Equation (1), using boundary and initial conditions presented in Section 2, can be presented as [5]:

$$T(X,t) = T_{\mathrm{w}} + \frac{Xh_0}{1+h_0}(T_{\mathrm{eff}} - T_{\mathrm{w}}) + \sum_{n=1}^{\infty} \exp[-\kappa_{\delta 0}\lambda_n^2 t][q_n + f_n h_0 (T_{\mathrm{eff}} - T_{\mathrm{w}})]\sin(\lambda_n X), \quad (15)$$

where $X = x/\delta_0$, $h_0 = h\delta_0/k_{\mathrm{l}}$, $\kappa_{\delta 0} = k_{\mathrm{l}}/(c_{\mathrm{l}}\rho_{\mathrm{l}}\delta_0^2)$, $q_n = \frac{1}{||v_n||^2}\int_0^1 (T_0(X) - T_{\mathrm{w}})\sin(\lambda_n X)\mathrm{d}X$, $f_n = \frac{1}{||v_n||^2}\int_0^1 f(X)\sin(\lambda_n X)\mathrm{d}X = -\frac{\sin\lambda_n}{||v_n||^2\lambda_n^2}$, $f(X) = -X/(1+h_0)$, $||v_n||^2 = \frac{1}{2}\left(1 - \frac{\sin 2\lambda_n}{2\lambda_n}\right) = \frac{1}{2}\left(1 + \frac{h_0}{h_0^2+\lambda_n^2}\right)$, λ_n are non-trivial solutions to the following equation $\lambda\cos\lambda + h_0\sin\lambda = 0$.

The solution to Equation (7), using boundary and initial conditions presented in Section 2, can be presented as [5]:

$$Y_{\mathrm{l},i}(t,x) = q_{Y0}\exp\left[D_{\mathrm{l}}\left(\frac{\lambda_0}{\delta_0}\right)^2 t\right]\cosh\left(\lambda_0\frac{x}{\delta_0}\right) + \sum_{n=1}^{\infty} q_{Yn}\exp\left[-D_{\mathrm{l}}\left(\frac{\lambda_n}{\delta_0}\right)^2 t\right]\cos\left(\lambda_n\frac{x}{\delta_0}\right) + \epsilon_i. \quad (16)$$

where $q_{Yn} = \frac{1}{||v_n||^2}\int_0^{\delta_0} u_0(x)v_n(x)\mathrm{d}x$, $u_0(x) = u(t=0) = Y_{\mathrm{l}0,i}(x) - \epsilon_i$,

$$v_n(x) = \begin{cases} \cosh\left(\lambda_0\frac{x}{\delta_0}\right) & n = 0 \\ \cos\left(\lambda_n\frac{x}{\delta_0}\right) & n \geq 1, \end{cases}$$

λ_n $(n \geq 0)$ are non-trivial solutions to the following equations:

$$\coth\lambda_0 = \frac{\lambda_0 D_{\mathrm{l}}}{|\dot{\delta}_{0e}|\delta_0}, \qquad \cot\lambda_n = -\frac{\lambda_n D_{\mathrm{l}}}{|\dot{\delta}_{0e}|\delta_0} \quad (n \geq 1).$$